

Seeing World Dynamics in a Nutshell

Qihong Shen^{1*}, Xuanyu Yi^{2*}, Mingbao Lin³, Hanwang Zhang²,
Shuicheng Yan^{3,1}, Xinchao Wang¹

¹ National University of Singapore ² Nanyang Technological University
³ Skywork AI

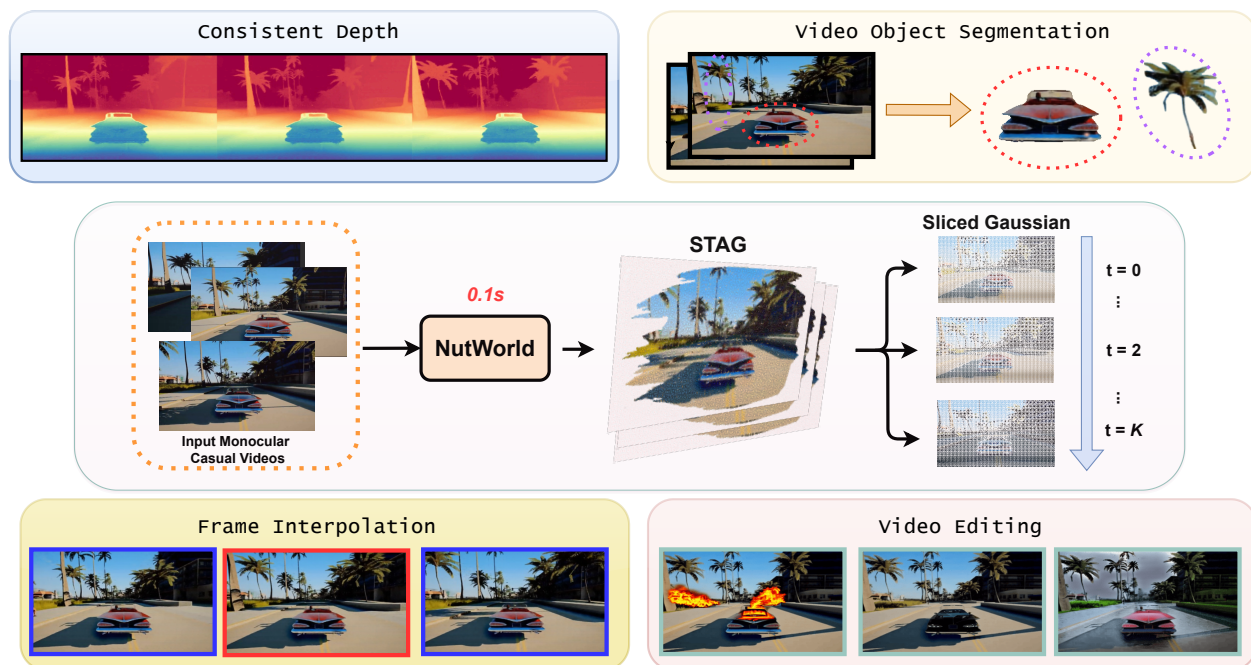


Figure 1. We introduce NutWorld, a *feed-forward* framework representing casual monocular videos parameterized by spatial-temporal aligned Gaussian (STAG), which empowers various video downstream processing tasks.

Abstract

We consider the problem of efficiently representing casually captured monocular videos in a spatially- and temporally-coherent manner. While existing approaches predominantly rely on 2D/2.5D techniques treating videos as collections of spatiotemporal pixels, they struggle with complex motions, occlusions, and geometric consistency due to absence of temporal coherence and explicit 3D structure. Drawing inspiration from monocular video as a projection of the dynamic 3D world, we explore representing videos in their intrinsic 3D form through continuous flows of Gaussian primitives in space-time. In this paper, we propose *NutWorld*, a novel framework that efficiently transforms monocular

videos into dynamic 3D Gaussian representations in a single forward pass. At its core, *NutWorld* introduces a structured spatial-temporal aligned Gaussian (STAG) representation, enabling optimization-free scene modeling with effective depth and flow regularization. Through comprehensive experiments, we demonstrate that *NutWorld* achieves high-fidelity video reconstruction quality while enabling various downstream applications in real-time. Demos and code will be available at <https://github.com/NutWorld/NutWorld>.

1. Introduction

Our natural world exhibits inherent dynamism—from rustling leaves swaying in the wind to clouds drifting across the sky and ocean waves rolling along the shore—where objects maintain their structural integrity while undergoing

*Equal Contribution

‡Work partially done in 2050 Research, Skywork AI

continuous spatiotemporal evolution. A fundamental objective in video processing [5, 65] is to enable machines to interpret such visual information, allowing recovery of both object geometry and motion patterns while preserving the spatiotemporal coherence intrinsic to human perception. This capability is crucial for numerous applications, ranging from autonomous driving [20, 34] and robotics [24, 25, 43] to augmented reality and content creation [2, 31, 61, 85], where an accurate understanding of dynamic scenes directly impacts system performance and user experience.

The current neural-based video representation [44, 58, 82] focuses predominantly on 2D and 2.5D techniques, treating videos as collections of spatiotemporal pixels [17, 91]. Although these discrete representations enable basic temporal modeling through pixel matching [60] and tracking [27, 81], they struggle to capture complex scene dynamics and maintain geometric consistency, particularly in challenging scenarios involving occlusions and non-rigid deformations [42, 44]. Moreover, these approaches inherently lack explicit 3D understanding, leading to unreliable spatial arrangements and limitations in novel view synthesis [40].

Drawing inspiration from monocular video as a projection of the dynamic 3D world, we investigate whether *videos can be represented in their intrinsic 3D form without per-scene optimization*. Recent advances in dynamic Gaussian Splatting [29] have shown unprecedented capabilities in dynamic scene reconstruction [16, 62, 75, 80], achieving high-fidelity rendering with explicit 3D representation and superior efficiency. By modeling videos as continuous flows of Gaussian primitives over time, we address the limitations of 2D representations while enabling efficient video processing. As shown in Figure 1, this paradigm treats space-time as an entirety and offers key advantages: each Gaussian functions as a flexible building block adapting to local geometric structures, enabling seamless representation of complex scenes across scales. Moreover, when embraced with dynamic attributes, these structured Gaussians naturally approximate the underlying spatiotemporal 4D volume of dynamic scenes, capturing intrinsic motions with demonstrated temporal consistency and facilitating various downstream tasks including novel view synthesis [40, 86], video editing [7, 49], and frame interpolation [14, 39].

However, transforming casually captured monocular videos to dynamic Gaussian representations *instantly (sec./frame)* presents several challenges: **(1) Unposed inputs.** Gaussian Splatting [29] and its variants [23, 87, 88] heavily rely on accurate camera poses obtained through Structure-from-Motion (SfM) [54, 66], which are typically unavailable for casual monocular videos. Without such pose guidance, current methods [4, 19, 35, 73] fail to disentangle camera motion from scene dynamics, resulting in deteriorated rendering quality and even collapsed reconstruction. **(2) Nonstructural Nature.** Most existing dynamic Gaus-

sian Splatting either leverage per-scene optimized deformation networks [16, 28, 32, 75, 79, 80] or adopt per-frame Gaussian generation [53] for dynamics modeling, both incompatible with our feed-forward prediction paradigm. The spatially unstructured property of Gaussian primitives further makes them prone to local minima in inverse rendering [10, 95], impeding feed-forward modeling of dynamic 3D scenes. **(3) Spatial Ambiguity.** The absence of multi-view supervision and initialization from SfM points significantly limits the spatial modeling capability of Gaussian Splatting, leading to ambiguous scale, depth collapse, and inconsistent spatial arrangements in reconstructed scenes.

To address the above challenges, we introduce *NutWorld* to efficiently transform monocular videos into dynamic Gaussian Splatting representations in a *single forward pass*. Our approach comprises three key components: (1) A structured spatial-temporal aligned Gaussian (STAG) representation in canonical space (Section 4.1), which enables feed-forward prediction while ensuring pose-free and scale-invariant modeling. (2) An optimization-free pipeline (Section 4.2) that learns spatial-temporal correspondence and continuous temporal dynamics across video frames, efficiently converting them into STAG representations. (3) Depth and flow regularization (Section 4.3) that incorporates calibrated monocular depth [78] and optical flow priors [76] to resolve spatial ambiguity and motion-appearance entanglement in the ill-posed monocular video setting [62, 69]. Through large-scale pre-training, *NutWorld* could process arbitrarily long videos while maintaining spatial-temporal consistency via segment-based inference (Section 4.4).

We conducted qualitative and quantitative experiments on RealEstate10K [94] and MiraData [26] to verify the representation efficacy of our proposed *NutWorld* in terms of video reconstruction. Moreover, our approach demonstrates compelling flexibility while maintaining real-time inference speed across various video downstream applications, including novel view synthesis, consistent depth estimation, video segmentation, as well as video editing and frame interpolation, suggesting its potential as a general-purpose video representation framework. The contributions and novelties of our paper are summarized as follows:

- We present the *first* framework to efficiently represent world dynamics in casually captured monocular videos as dynamic Gaussian Splatting in a *single forward pass*.
- Our *NutWorld* framework incorporates the STAG representation, elaborated network for feed-forward reconstruction, and effective regularization strategies for spatial and temporal coherent recovery from casual videos.
- Extensive experiments on video reconstruction and various downstream tasks demonstrate the spatial-temporal coherence and the versatility of *NutWorld*.

2. Related Work

Dynamic 3D scene reconstruction. Dynamic scenes, with moving objects and varying lighting conditions, require models that can handle temporal variations and motion in 3D space. While early works extended NeRF [40] to dynamic scenes [46–48] through temporal representations [48] and deformable fields [6], they remain computationally intensive due to MLPs and volume rendering [41]. Recent dynamic 3D Gaussian Splatting addresses this limitation by using deformable 3D Gaussian [28, 32, 75, 80] or anisotropic 4D Gaussian [16, 79], enabling efficient rendering through tile-based rasterization [29]. Among them, concurrent works [33, 62, 69, 71] have demonstrated dynamic scene reconstruction from unposed monocular videos. However, they rely on computationally intensive per-scene optimization, making them impractical for real-world applications. In contrast, our NutWorld focuses on neural video representation (NVR) without the availability of camera poses, specifically addressing the challenge of explicitly representing monocular videos rather than dynamic 3D scene reconstruction. Moreover, it employs a *feed-forward* approach that enables fast inference with high reconstruction quality and temporal consistency, distinguishing itself from tedious optimization-based 3D reconstruction paradigms.

Feed-Forward Gaussian Splatting. Recent advance in large-scale 3D scene datasets [36, 37, 94] has enabled feed-forward Gaussian approaches [8, 9, 55, 74, 84, 90, 92], which excel in efficiency and sparse view reconstruction. PixelSplat [8] and LatentSplat [74] employ the epipolar transformer [21, 72] to establish cross-view correspondences and predict 3D Gaussians from multi-view image features, while MVSPat [9] utilizes cost volumes to jointly predict depth and Gaussian parameters. Alternatively, GS-LRM [92] and Long-LRM [96] consider Gaussian Splatting reconstruction as a sequence-to-sequence translation task, employing transformer-based [67] or hybrid [12] architectures to regress Gaussian primitives. Although these methods address static 3D reconstruction, NutWorld is the *first* to represent dynamic scenes from unposed monocular videos.

3. Preliminary: Dynamic Gaussian Splatting

Dynamic Gaussian Splatting [16, 28, 32, 75, 79, 80] is an explicit 4D neural representation for reconstructing dynamic 3D scenes from multi-view videos through differentiable rasterization [29]. Dynamic Gaussian $\{\mathcal{G}_i, \mathcal{D}_i(t)\}$ decouples dynamic scenes into a static canonical 3D Gaussian \mathcal{G}_i and a deformation motion field \mathcal{D}_i to account for temporal variations in 3D space. Specifically, the static 3D Gaussian \mathcal{G}_i is composed of a 3D center $\mu \in \mathbb{R}^3$, 3D scale $s \in \mathbb{R}^3$, associated color $c \in \mathbb{R}^3$, opacity $\alpha \in \mathbb{R}$, and rotation quaternion $q \in \mathbb{R}^4$. For the deformation fields $\mathcal{D}_i(t) = \{\mu_i(t), q_i(t), \alpha_i(t)\}$, the deformable attributes and

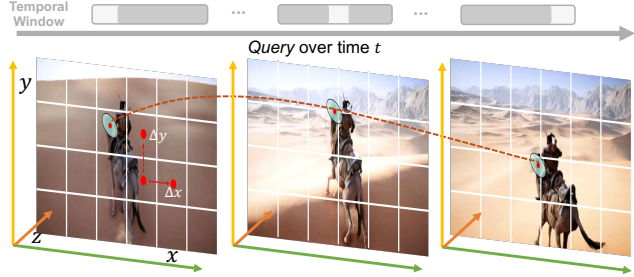


Figure 2. The illustration of STAG to represent dynamic scenes.

their parameterizations vary across different approaches but are generally limited to the center position μ_i , rotation q_i , and opacity α_i , with other attributes remaining independent of time. When representing the scene at time t , each dynamic Gaussian is temporally sliced into 3D space by applying its corresponding deformation field $\mathcal{D}_i(t)$ to yield an static Gaussian primitive, e.g., with deformed position $\hat{\mu}_i = \mu_i + \mu_i(t)$, which can then be efficiently rendered into 2D images via tile-based rasterization pipeline.

4. Methodology

In this section, we present a framework for efficiently representing world dynamics from monocular video in a *feed-forward manner*. As shown in Figure 3, we first introduce our Spatial-Temporal Aligned Gaussian Splatting (STAG) representation (Section 4.1). To enable the mapping of videos to STAG in a single forward pass, we detail our transformer-based network (Section 4.2), which operates with calibrated depth and flow priors (Section 4.3). Finally, we discuss the overall training objectives and protocols for processing long video segments (Section 4.4).

4.1. Spatial-Temporal Aligned Gaussian

Canonical camera space. Given an unposed monocular video, we employ an orthographic camera coordinate system instead of an absolute 3D world coordinate system. This choice is motivated by two key challenges: the difficulty of obtaining coherent camera trajectories in dynamic scenes [45, 54, 66, 68, 70], and the inherent scale ambiguity in feed-forward 3D reconstruction models [8, 9, 90], where perspective projection couples object scale with its distance from camera. By adopting orthographic projection with a fixed pose along the z axis, we eliminate the necessity for explicit camera pose estimation while modeling both camera and object motion without scale ambiguity in a unified canonical space. We provide a detailed implementation of the orthographic rasterization pipeline in the *Appendix*.

Structured Dynamic Gaussian. To overcome the unstructured nature in dynamic Gaussian Splatting and facilitate neural network integration, we introduce Spatial-Temporal Aligned Gaussian Splatting (STAG) in the canonical cam-

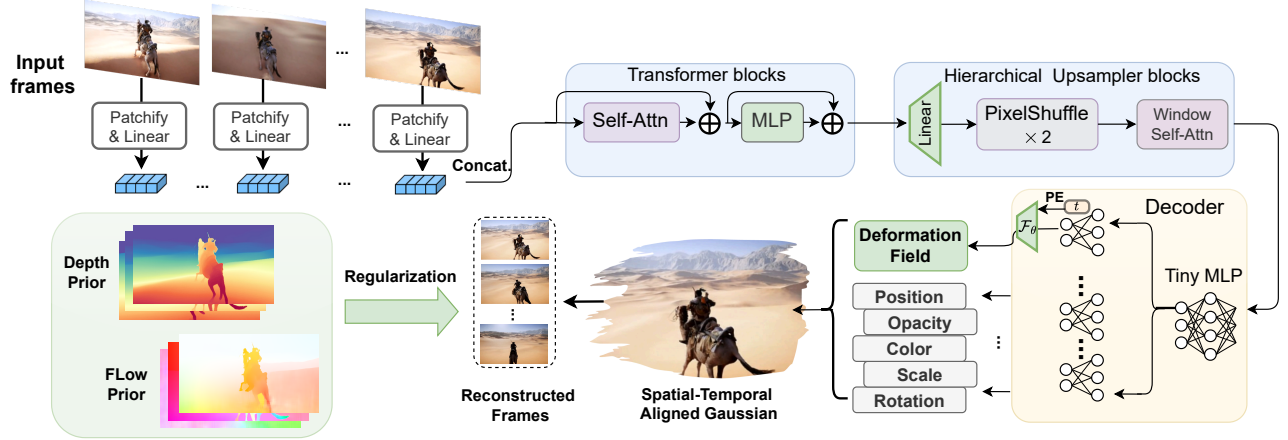


Figure 3. **Overview of NutWorld.** We directly predict STAG in a canonical space from sparse input frames via a transformer-based reconstruction model, where calibrated depth and flow priors are leveraged to avoid depth ambiguity and motion uncertainty.

era space. STAG constrains each dynamic Gaussian to a specific pixel location and timestamp, in contrast to the previous approach of predicting unconstrained Gaussians with deformable fields across orthogonal space-time. Formally, for an input frame F_k with normalized timestamp $t_k \in [0, 1]$, we compute a Gaussian feature map $\mathcal{E}^k \in \mathbb{R}^{U \times V \times T}$, where U and V represent spatial dimensions, and T denotes the channel dimension. Each T -dimensional pixel is decoded into a 3D Gaussian with an associated deformation field $\{\mathcal{G}_i, \mu_i(t)\}^*$ in a pixel-aligned manner [8, 63].

Given a pixel at coordinates (u, v) in the feature map \mathcal{E}^k , we define its corresponding 3D Gaussian center μ^k through unprojection along the corresponding ray: $\mu^k = (u + \Delta_x, v + \Delta_y, d)$, where Δ_x and Δ_y are bounded offsets decoded from \mathcal{E}^k , maintaining pixel-level correspondence with local position refinement. The depth value d specifies the z -coordinate of μ^k along the camera’s viewing axis. To model temporal dynamics, for frame rendering at timestamp t_j , we deform each static Gaussian center μ^k during frame rendering at timestamp t_j using the predicted deformation field $\mu^k(t)$:

$$\hat{\mu}^k = \mu^k + \mu^k(t_j) \mathbb{1}(t_k, t_j), \quad (1)$$

where $\mathbb{1}(t_k, t_j)$ is a temporal slicing indicator function defined as:

$$\mathbb{1}(t_k, t_j) = \begin{cases} 0, & \text{if } t_j = t_k \text{ (reference frame),} \\ 1, & \text{otherwise (non-reference frame).} \end{cases} \quad (2)$$

As shown in Figure 2, the temporal slicing function $\mathbb{1}(t_k, t_j)$ modulates the deformation field $\mu^k(t_j)$ based on the temporal relationship between the rendering timestamp t_j and the Gaussian’s reference timestamp t_k . For $t_j = t_k$, the deformation is suppressed ($\mathbb{1}(t_k, t_j) = 0$), preserving

*Note that based on our empirical observation, we simplify the deformation modeling by considering only the center position, such that the deformation field reduces to $\mathcal{D}_i(t) = \mu_i(t)$.

the original Gaussian position μ^k to maintain spatial alignment. When $t_j \neq t_k$, the deformation field $\mu^k(t_j)$ is activated to adjust μ^k , allowing the Gaussian center to adapt to temporal differences.

4.2. Encapsulate Dynamics within “Nutshell”

In this section, we introduce the transformer-based model in NutWorld to transform unposed monocular videos into the proposed STAG. Formally, given an input sequence of K video frames $\{F_k, t_k\}$, where each frame $F_k \in \mathbb{R}^{H \times W \times 3}$ is associated with a normalized timestamp $t_k \in [0, 1]$, we define NutWorld as an inverse mapping function Θ :

$$\{\mathcal{G}_i, \mu_i(t)\} = \Theta(\{F_k, t_k\}). \quad (3)$$

This mapping generates a set of STAGs $\{\mathcal{G}_i, \mu_i(t)\}$ that can be rendered into arbitrary frames ($M \geq K$) through temporal interpolation of the deformation field. Specifically, **Transformer-based Encoder.** For each input frame $F_k \in \mathbb{R}^{H \times W \times 3}$, we augment pixels by concatenating their RGB values with corresponding depth coordinates d_k^* along the channel dimension, obtained from a pre-trained depth estimation model [78]. The augmented frames are first split into non-overlapping patches of size $p \times p$ using convolutions, which are then linearly transformed and concatenated across all frames to generate transformer input tokens. Notably, our architecture eliminates the need for explicit positional embeddings as used in ViT [1, 15], since depth coordinates inherently encode spatial information. The transformer blocks, comprising self-attention [67] and MLP layers, process these concatenated tokens to capture spatiotemporal correspondence and produce encoded features $\mathcal{E}_0 \in \mathbb{R}^{K \times h \times w \times C}$, where $h = H/p$ and $w = W/p$ denote the spatial resolution and C denotes the feature dimension. To ensure sufficient STAGs for casual videos, we leverage a hierarchical upsampling network [77, 92] that progressively expands the spatial resolution of the encoded

feature \mathcal{E}_0 . Each upsampler block first expands the feature dimension by a factor of 4 through a linear layer, followed by a PixelShuffle [57] layer that doubles the spatial resolution. The resulting features are then processed by a local attention layer with window size \mathcal{W} , which balances computational efficiency and spatial-temporal feature aggregation:

$$\begin{aligned}\hat{\mathcal{E}}_{j-1} &= \text{PixelShuffle}(\text{Linear}(\mathcal{E}_{j-1}), 2), \\ \mathcal{E}_j &= \text{WindowAttn}(\hat{\mathcal{E}}_{j-1}, \mathcal{W}).\end{aligned}\quad (4)$$

After cascading such blocks n times, the final feature map \mathcal{E}_n achieves a spatial resolution of $(U, V) = (2^n h, 2^n w)$.

STAG Decoder. The proposed decoder predicts both static Gaussian attributes and their deformable field from the up-sampled feature map \mathcal{E}_n . For decoding static 3D Gaussian, we employ a shared MLP with specialized sub-heads to predict each Gaussian attribute: center position μ , opacity α , scale s , rotation q , and color c is RGB value $\in [-1, 1]^3$. Given our fixed canonical camera setup, we omit view-dependent effects in color prediction. Each attribute utilizes specific activation functions following established practices [8], with details provided in the *Appendix*.

To model the deformation field $\mu(t)$ as a continuous function of time, we encode the timestamp t using sinusoidal positional encoding followed by a learnable linear projection. The encoded time features are then processed by an MLP to enable differentiable temporal interpolation:

$$\mu(t) = \mathcal{F}_\theta(\text{Linear}(\gamma_n(t)), \mathcal{E}_n(k, u, v)), \quad (5)$$

where \mathcal{F}_θ represents an MLP with learnable parameters θ . A \tanh activation is applied to the output, constraining the deformation within the bounds $[-b, b]^3$. The function $\gamma(t) = (\sin(2^k \pi t), \cos(2^k \pi t))_{k=0}^{L-1}$ represents the sinusoidal expansion of order L , which enhances the network’s capacity to capture high-frequency components effectively.

4.3. Calibrated 2D Priors Regularization

Learning spatially-aware STAGs solely from monocular videos is inherently ill-posed due to depth ambiguity and motion uncertainty. Therefore, we leverage off-the-shelf foundation models [76, 78] to recover spatial relationships and temporal motion through calibrated depth and flow priors, respectively. Under the orthographic projection, the movement of STAG along the xy-coordinates directly corresponds to optical flow magnitude, whereas depth-related loss exclusively affects the z-coordinate, further facilitating the incorporation of those 2D priors.

Depth Regularization. To enhance robustness against scale and shift variations in depth rendering, we employ a scale and shift invariant loss [3, 52]. This loss function computes optimal scaling β and shifting γ factors that align the rendered depth d with the pseudo depth d^* estimated by the depth prior model [78]. The optimal values for β and γ

are obtained by minimizing the squared error between the scaled rendered depth and the pseudo depth, as follows:

$$\begin{aligned}\beta, t &= \arg \min_{\beta, \gamma} \sum_i M_i (\beta \cdot d_i + \gamma - d_i^*)^2, \\ \mathcal{L}_{\text{depth}} &= \sum_{i=1}^{H \times W} |\tilde{d}_i - d_i^*| / \sum M, \quad \tilde{d}_i = \beta \cdot d_i + \gamma.\end{aligned}\quad (6)$$

Here, M is an outlier mask where $M_i = 0$ for the top 10% values in each depth map and $M_i = 1$ otherwise, mitigating noise in the estimated pseudo depth d^* . This depth supervision effectively regularizes the training, making it robust for predicting relative depth in scenes.

Flow Regularization. We extract global STAG trajectories by leveraging frame-to-frame optical flow associations [76]. In contrast to previous methods that solely employ iterative optimization between adjacent frames, our feed-forward framework utilizes global trajectory supervision to ensure consistent motion in a single forward pass.

For each STAG, we define its estimated pseudo-trajectory $\bar{\mu}^*(t)$ across K video frames. This trajectory is derived by sequential queries to the pre-computed optical flow field between adjacent frames, represented by a global flow matrix \mathbf{F} :

$$\mathbf{F} = \begin{pmatrix} (0, 0, \dots, 0) & \mathbf{f}_{1 \rightarrow 0} & \mathbf{f}_{2 \rightarrow 1} + \mathbf{f}_{1 \rightarrow 0} & \dots & \sum_{k=1}^{K-1} \mathbf{f}_{k \rightarrow k-1} \\ & \mathbf{f}_{0 \rightarrow 1} & (0, 0, \dots, 0) & \mathbf{f}_{2 \rightarrow 1} & \dots & \sum_{k=2}^{K-1} \mathbf{f}_{k \rightarrow k-1} \\ \mathbf{f}_{0 \rightarrow 1} + \mathbf{f}_{1 \rightarrow 2} & \mathbf{f}_{1 \rightarrow 2} & (0, 0, \dots, 0) & \dots & \sum_{k=3}^{K-1} \mathbf{f}_{k \rightarrow k-1} \\ \vdots & \vdots & \vdots & \ddots & \vdots \\ \sum_{k=1}^{K-1} \mathbf{f}_{k-1 \rightarrow k} & \sum_{k=2}^{K-1} \mathbf{f}_{k-1 \rightarrow k} & \sum_{k=3}^{K-1} \mathbf{f}_{k-1 \rightarrow k} & \dots & (0, 0, \dots, 0) \end{pmatrix} \quad (7)$$

The global flow matrix \mathbf{F} is structured as a $K \times K$ matrix, where each entry $\mathbf{F}_{i,j}$ is structured as a vector of length $(U \times V)$ represents the 2D cumulative motion of each Gaussian from frame j to frame i . The matrix structure is asymmetric: upper triangular entries encode cumulative backward flow $\mathbf{f}_{k \rightarrow k-1}(\bar{\mu}_i)$, while lower triangular entries contain cumulative forward flow $\mathbf{f}_{k \rightarrow k+1}(\bar{\mu}_i)$. Here, $\bar{\mu}_i$ denotes the projected 2D coordinates of the i -th Gaussian in frame k . For notational clarity, we omit the explicit flow query operations in the matrix entries.

Using the global flow matrix, we regularize the deformation field $\mu(t)$ by comparing its 2D projection $\bar{\mu}(t)$ against the estimated global trajectories $\mu^*(t)$ across K frames:

$$\mathcal{L}_{\text{flow}} = \sum_{i=1}^{K \times U \times V} \sum_{k=0}^{K-1} \|\bar{\mu}_i(t_k) - \mu_i^*(t_k)\|_1, \quad (8)$$

where $\|\cdot\|_1$ denotes the L1 norm. An outlier filtering strategy is also applied to calibrate the flow prior (see *Appendix*



Figure 4. Qualitative comparison of video reconstruction using our NutWorld and other optimization-based methods.

Method	PSNR \uparrow	SSIM \uparrow	LPIPS \downarrow	Inference Time	GPU Mem.	FPS
4DGS [75]	17.59	0.5725	0.5393	\sim 40 mins	10G	145
RoDynRF [38]	24.63	0.7152	0.3927	$>$ 24 hours	24G	$<$ 0.01
CoDeF [44]	26.35	0.8045	0.2714	\sim 30 mins	10G	8.8
Splatter-a-Video [62]	24.85	0.7413	0.3523	\sim 30 mins	10G	149
Ours	29.18	0.9015	0.1415	1.8 seconds	4G	450

Table 1. Quantitative comparison with state-of-the-art methods. GPU Memory is measured in GB and FPS indicates rendering frame rate.

for flow calibration details). This flow loss enforces consistency between the predicted trajectories and the reference paths derived from optical flow, enabling NutWorld to learn coherent motion patterns from casually captured videos.

4.4. Training and Inference

Overall objective. During the training phase, we render RGB frames from $K = 6$ sparsely sampled frames and interpolate $M = 10$ intermediate frames for dense temporal supervision. Our training objective comprises three terms:

$$\mathcal{L} = \mathcal{L}_{\text{MSE}} + \lambda_{\text{flow}}\mathcal{L}_{\text{flow}} + \lambda_{\text{depth}}\mathcal{L}_{\text{depth}}, \quad (9)$$

where \mathcal{L}_{MSE} is the mean square error loss between the rendered and ground truth RGB frames. $\mathcal{L}_{\text{flow}}$ and $\mathcal{L}_{\text{depth}}$ denote the calibrated regularization term, respectively. The coefficients λ_{flow} and λ_{depth} balance the contribution of each term.

Segment-based long video inference. To handle casual videos with hundreds of frames, we propose a simple but effective segment-based strategy during inference. The input video is divided into overlapping segments, where the adjacent segments share one frame. Due to our pixel-level spatial-temporal representation, Gaussian trajectories can be seamlessly propagated across segments through these shared frames, enabling NutWorld to process arbitrarily long videos while maintaining spatial-temporal consistency. The details of segment-based inference is in *Appendix*.

5. Experiment

5.1. Experimental Setup

Training Dataset. NutWorld is pre-trained on MiraData [26] and RealEstate10K [94]. MiraData is a high-quality video dataset consisting primarily of 3D engine-generated scenes and movie clips with diverse motion patterns. The RealEstate10K dataset contains indoor house tour videos that showcase various architectural scenes and camera movements \dagger . During pre-processing, we segment the original videos into video cubes, each containing 10 consecutive frames as the basic processing unit. Detailed information on the description of the dataset, preprocessing, and splitting of trains is provided in the *Appendix*.

Implementation Details. NutWorld is trained on 32 NVIDIA A100 (80GB) GPUs with a batch size of 256 for around 4 days. To improve computational efficiency, we integrate Flash-Attention-v2 [11, 13], gradient checkpointing [59], and mixed-precision training with BF16 [89]. The orthographic camera coordinates are bounded to $[-1, 1]$ along the x and y axes and to $[0, 1]$ along the z axis. The input frames are resized to 512×288 to preserve the aspect ratio. We adopt a two-phase training strategy: a static phase using single frames ($K = 1$) with window size $\mathcal{W} = 576$, followed by a dynamic phase where we initialize from the

\dagger Unlike previous Generalizable 3DGS approaches [8, 9, 90], we treat RealEstate10K as a pure video dataset rather than a multi-view 3D scene dataset, thus not utilizing the COLMAP-calibrated camera poses

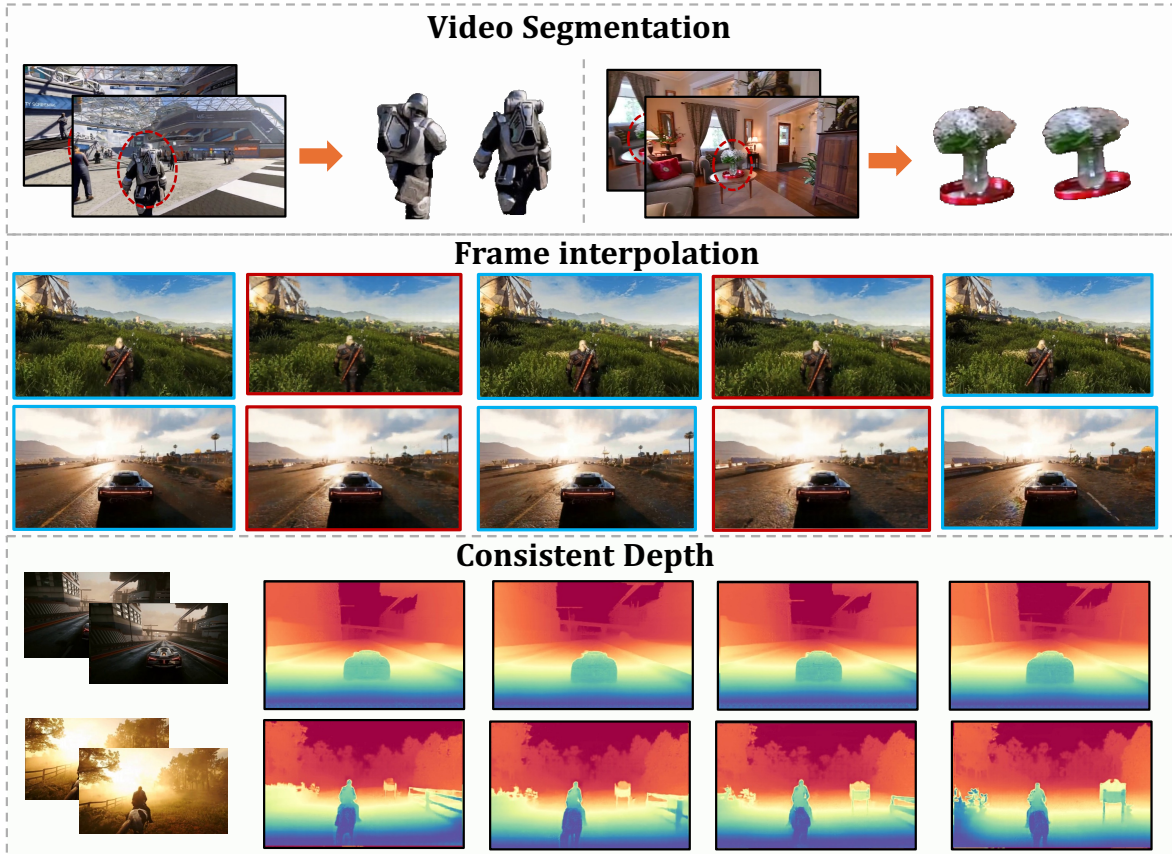


Figure 5. Qualitative results in various downstream tasks, including video segmentation, editing, frame interpolation and consistent depth estimation. More visualization results for each task are presented in *Appendix*.

static weights and expand the window to $\mathcal{W} = 3456$ to allow spatio-temporal attention in the hierarchical upsampler. Additional training details, including hyper-parameters and network architecture, are provided in the *Appendix*.

5.2. Video Reconstruction

Experimental Protocol. We evaluated the video reconstruction performance of NutWorld on 50 randomly selected test video clips from RealEstate10K and MiraData, both with a default length of 90 frames via standard reconstruction quality metrics (PSNR, SSIM, and LPIPS [93]). As there are currently no other feed-forward dynamic Gaussian approaches, we compared with optimization-based methods including Splatter-a-Video (SaV) [62], 4DGS [75], RoDynRF [38] and CoDeF [44] as the most relevant baselines. For fair comparison, all methods incorporate the confined canonical space, depth and flow supervision. We used the official implementations for most methods while SaV was reproduced according to the implementation details provided in their paper.

Comparison with Baselines. We evaluate NutWorld’s representation effectiveness through both qualitative and quantitative experiments on video reconstruction. As shown

in Figure 4, our pre-trained NutWorld effectively captures spatial details and temporal dynamics, outperforming both Gaussian-based SaV [62] and NeRF-based CoDeF [44] in reconstruction quality. This superior performance can be attributed to STAG’s elaborated deformable field and positional constraints, which provide more expressive and robust temporal modeling capabilities compared to SaV’s Fourier series and CoDeF’s 2D canonical representation. Furthermore, as evidenced in Table 1, NutWorld achieves the best of both worlds in reconstruction quality and computational efficiency. Notably, NutWorld reconstructs a 90-frame video in just 1.8 seconds, achieving a $1000\times$ speedup over optimization-based methods. Equipped with segment-based inference that limits the number of Gaussians per segment, NutWorld achieves a rendering speed of 450 FPS, substantially surpassing SaV’s 149 FPS, which requires around 2×10^6 Gaussians for the same video.

5.3. Video Downstream Tasks

Large-scale pretrained NutWorld empowers video applications including object segmentation, frame interpolation, video editing, novel view synthesis, and consistent depth prediction. We present representative qualitative results in

Figure 5, with additional results provided in the *Appendix*.

Video object segmentation. The explicit nature of STAG allows us to propagate object masks in a certain frame to subsequent frames. Specifically, the corresponding STAGs in the object mask can be explicitly selected in the first frame, as demonstrated in previous training free Gaussian segmentation methods [22, 56]. As NutWorld predicts coherent deformation $u_i(t)$ for each Gaussian over time, object masks in subsequent frames can be rendered from the STAGs selected initially. In particular, this capability emerges as a by-product without task-specific training [44, 62].

Frame interpolation. The continuous trajectories learned for STAGs, regularized by calibrated optical flow, enable temporal interpolation of scene dynamics at arbitrary FPS. These interpolated STAGs, with smoothly varying dynamic attributes, facilitate intermediate frame rendering, a capability beyond the scope of per-frame methods [53].

Consistent depth prediction. The calibrated depth regularization prevents depth collapse while maintaining temporally coherent spatial configurations in scene geometry. Additionally, NutWorld demonstrates potential for distilling other image features, such as SAM [30] and CLIP [51], which we consider a promising direction for future work.

Video editing. By integrating with a MLLM-guided editing model [18], NutWorld enables precise frame-level painting and stylization by optimizing the sliced STAG representation. These edits propagate temporally while maintaining visual coherence throughout the video sequence. The visualization results are provided in the *Appendix*.

Novel view synthesis. NutWorld achieves novel view synthesis within practical bounds by incorporating depth priors to mitigate spatial ambiguity. Camera extrinsic adjustment enables novel view rendering, while camera intrinsic manipulation allows for effects such as dolly zoom. Please refers to *Appendix* for the visualization results.

6. Ablation Study

We analyze NutWorld’s design choices through ablation studies on the 50 selected video clips. As shown in Table 2, our experiments demonstrate that discarding any component from the multi-component pipeline leads to significant performance degradation. Specifically:

Ablations on STAG representation. To validate the effectiveness of STAG representation, we perform an ablation by loosening its positional constraints. Following [64], we implement a less constrained variant where Gaussian positions are predicted with only \tanh activation, limiting their range to $[-1, 1]$. As shown in Table 2, this loosened constraint leads to significantly degraded performance by $10dB$ decrease in PSNR, with slower convergence, blurred artifacts and unstable optimization behavior. These results demonstrate the necessity of structured positional constraints, as

Method	PSNR \uparrow	SSIM \uparrow	LPIPS \downarrow
w/o Flow Loss	26.39	0.8345	0.2482
w/o Depth Loss	28.15	0.8751	0.1858
w/o STAG	19.58	0.6255	0.4713
Ours ($n = 2$)	29.18	0.9015	0.1415
Ours ($n = 3$)	31.15	0.9266	0.1385

Table 2. Ablation study on component-wise contribution. n represents the number of upsampler blocks.

the unconstrained Gaussians introduce additional spatial ambiguity during alpha compositing. In contrast, STAG’s localized positional constraints provide explicit spatial and temporal correspondence, enabling efficient optimization and high-quality rendering.

Ablations on depth prior. To evaluate the depth prior (Eq. 6), we trained the NutWorld variant without depth supervision in Figure 6(a) for comparison, which reveals that the variant w/o depth tend to lost spatial arrangement and converges to a collapsed shortcut instead, i.e. all STAGs are splattered onto a single z plane. Furthermore, quantitative experiments in Table 2 reveal that removing the depth prior leads to a degraded rendering quality, as evidenced by the decrease in PSNR from $29.18dB$ to $28.15dB$. These results highlight the necessity of depth prior to address the spatial ambiguity in NutWorld.

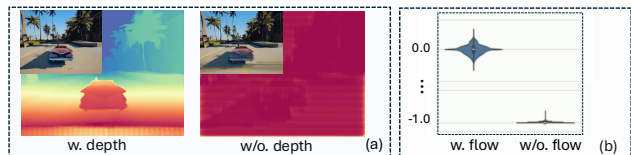


Figure 6. Qualitative ablation on 2D prior regularization.

Ablations on flow prior. To evaluate the flow prior (Eq. 8), we trained a NutWorld variant without flow supervision for comparison. The distribution of the deformation field $\mu(t)$ across $K = 6$ frames is visualized in Figure 6(b) via a violin plot. Without flow supervision, the model exhibits large deformation values with low variance, causing STAGs to deviate from the canonical space in non-reference frames as defined in Eq. 2. This indicates that the variant w/o flow tends to learn an undesirable shortcut by representing each frame with independent STAGs, leading to temporal discontinuity. In contrast, with flow supervision, the distributions are centered near zero with appropriate variance, demonstrating that NutWorld could recover temporal motion through the flow prior, which effectively prevents such shortcut behavior. Additionally, quantitative experiments in Table 2 show that temporal discontinuity leads to inferior reconstruction quality, especially for complex motions.

7. Conclusion

In this paper, we introduce NutWorld, a novel framework for efficiently representing casual monocular videos through dynamic Gaussian Splatting. By introducing the structured STAG representation and incorporating effective depth and flow regularization, our approach successfully tackles several fundamental challenges in monocular video representation, achieving both spatial and temporal coherence without per-scene optimization. Comprehensive experiments demonstrate that NutWorld not only achieves high-fidelity video reconstruction in real-time but also enables various downstream applications. In the future, distilling rich visual features (e.g., SAM, CLIP) into our STAG representation and adapting our representation paradigm for video generation tasks are promising directions to explore.

Seeing World Dynamics in a Nutshell

Supplementary Material

The *Appendix* is organized as follows:

- **Appendix 1:** provides additional details about the Nutworld pipeline, including the implementation of orthographic rasterization, Gaussian decoder, flow prior calibration, and segment-based inference.
- **Appendix 2:** provides further details on experiment design and model configuration.
- **Appendix 3:** presents additional experimental results on video reconstruction and downstream tasks.
- **Appendix 4:** discuss the limitations and potential future directions of NutWorld.

1. Implementation Details

Orthographic rasterization. Orthographic projection is leveraged to circumvent the necessity for explicit camera pose estimation in our setting. Specifically, we employ a fixed orthographic camera model and modify the EWA projection [97] from perspective to orthographic in Gaussian rasterization. The EWA projection in original rasterization is formulated as:

$$\Sigma' = JW\Sigma W^T J^T, \quad (10)$$

where J represents the Jacobian matrix of the projective transformation. In the case of perspective projection, the Jacobian J is formulated as:

$$(u, v) = (f_x \cdot x/z + c_x, f_y \cdot y/z + c_y),$$
$$J = \frac{\partial(u, v)}{\partial(x, y, z)} = \begin{pmatrix} f_x/z & 0 & -f_x \cdot x/z^2 \\ 0 & f_y/z & -f_y \cdot y/z^2 \end{pmatrix}. \quad (11)$$

In contrast, for orthographic projection, the EWA projection is modified as follows:

$$(u, v) = (f_x \cdot x + c_x, f_y \cdot y + c_y),$$
$$J = \frac{\partial(u, v)}{\partial(x, y, z)} = \begin{pmatrix} f_x & 0 & 0 \\ 0 & f_y & 0 \end{pmatrix}. \quad (12)$$

In this formulation, the near and far planes are set to 0 and 1, respectively, constraining the z axis within this range. Additionally, the x and y axes are constrained to $[-1, 1]$ to facilitate structured prediction.

STAG Parameterization. The parameterization of output parameters significantly impacts the model’s convergence, despite STAG provides a relatively structured Gaussian representation. For reproducibility, we provide detailed configuration of the STAG decoder parameterization in Table 3. Common activation functions such as sigmoid, softplus, and normalize are employed for most static Gaussian attributes, following previous works [8, 64, 77]. For

the spatial aligned 3D Gaussian position, we predict it as $\mu = (u + \Delta_x, v + \Delta_y, d)$, where u and v are the aligned 2D pixel positions within the orthographic space, and both Δ_x and Δ_y are constrained using the tanh activation. For the depth value d , the z axis in $[0, 1]$ is divided into 20 discrete bins. A discrete distribution is predicted over these bins, and the expectation is computed to robustly predict the depth value d . For the deformable fields $\mu(t)$, the query timestamp t is represented as $L = 10$ sinusoidal expansions. The output of \mathcal{F}_θ remains unbounded, allowing invisible Gaussians to be driven out of the view space as needed.

Attribute	parameterization
Position (static)	$x, y : \text{map} + \text{max} \cdot \tanh(\cdot)$
Position (dynamic)	unbounded
Depth	bin regression with softmax
Scale	$0.1 \cdot \text{softplus}$
Rotation	normalize
Opacity	sigmoid
RGB	sigmoid

Table 3. Detailed STAG parameterization.

Flow Prior Calibration. The estimated global optical flow between video frames often contains noise, which can hinder model convergence during training. To mitigate these noises, we employ a calibration strategy for the flow regularization loss $\mathcal{L}_{\text{flow}}$. Specifically, when a STAG moves out of the view space, we set the corresponding flow mask value $M_{i,k} = 0$. Additionally, we filter out flows with the top 20% motion magnitudes as outliers. With these adjustments, the calibrated flow regularization loss is expressed as:

$$\mathcal{L}_{\text{flow}} = \sum_{i=1}^{K \times U \times V} \sum_{k=0}^{K-1} M_{i,k} \|\bar{\mu}_i(t_k) - \mu_i^*(t_k)\|_1, \quad (13)$$

This calibration ensures that only reliable motion information contributes to the training process, reducing the impact of noise and extreme outliers, encouraging the model to learn coherent motion patterns effectively.

Segment-based inference. We adopt a segment-based inference approach to transform long casual videos into

STAG representations. This strategy processes video sequences using a sliding window mechanism, where each window contains one overlapping frame. Temporal coherence between segments is maintained through spatially aligned Gaussians in the overlapping frames shared by adjacent segments. The coherence is achieved through token-wise correspondence, as spatial positions in STAG directly correspond to identical pixel locations. Through quantitative comparison shown in Table.1 in the manuscript, we further demonstrate that this segment-based inference strategy not only efficiently processes video segments in parallel but also maintains a manageable number of Gaussians for each segment due to the slicing window design. In contrast, SaV [62] directly uses millions of Gaussians to represent entire frames, resulting in significantly longer rendering times per frame.

2. Experiment Configuration

Network Configuration. As illustrated in Table 4, the transformer-based encoder processes input frames at 288×512 resolution, with concatenated RGB and depth channels. The architecture comprises 10 attention layers with 12 heads and 768-dimensional features, operating on 16×16 patches. The hierarchical upsampler incorporates 3 blocks, each containing 2 attention layers with a window size of 3456. Through these blocks, the channel dimension progressively decreases from 768 to 64, while spatial resolution doubles at each stage. With $n = 2$ upsampler blocks, our model processes $K = 6$ input frames to produce feature maps of spatial resolution $(U, V) = (128, 72)$, generating 55,296 dynamic Gaussians. The STAG decoder implements a lightweight MLP with a single 1024-dimensional hidden layer, utilizing attribute-specific activation functions: linear for position, \tanh for dynamics, *Softplus* for scale, normalization for rotation, and *Sigmoid* for opacity and color.

Dataset Settings. NutWorld is pre-trained on MiraData [26] and RealEstate10K [94]. For MiraData, we utilize its middle version containing approximately 34K video clips, each with a duration of about 2 minutes. To ensure data quality, we performed rigorous filtering by removing clips containing gaming pop-ups, black screens, and other artifacts, resulting in a curated dataset of 22K video clips [83]. The dataset is split randomly with a 95:5 ratio for training and testing. For RealEstate10K, unlike previous Generalizable 3DGS approaches [8, 9, 90], we treat it as a pure video dataset rather than a multi-view 3D scene dataset, without utilizing COLMAP-calibrated camera poses. This dataset is similarly split with a 95:5 training-testing ratio. For evaluation, we randomly selected 40 videos from the MiraData test set and 10 from the RealEstate10K test set for both qualitative and quantitative comparison.

3. More Experiments Results

Due to limited space in the manuscript, we provide more qualitative results on video reconstruction, object segmentation, frame interpolation, editing, novel view synthesis and depth prediction in the following figures. Note that we don't claim that NutWorld achieves state-of-the-art performance across all these downstream tasks. Instead, our focus is on demonstrating NutWorld as a versatile video representation framework with broad applicability and adaptability. We believe that with task-specific adaptations, NutWorld has the potential to compete with specialized state-of-the-art methods in these individual video domains. **Please refer to the attached material for video visualization.**

4. Limitations

While our NutWorld framework demonstrates significant advances in spatial-temporal video modeling and rendering efficiency, several limitations warrant discussion. (1) The framework's reliance on depth and optical flow priors makes its performance inherently dependent on external models, which may not generalize effectively to challenging scenarios involving complex motion or suboptimal lighting conditions. (2) While the segment-based inference strategy enables accelerated rendering, it introduces a trade-off between processing speed and global temporal consistency by prioritizing localized frame segments over the complete video sequence. (3) Despite achieving substantial runtime efficiency, the framework's training process remains computationally intensive, potentially limiting its deployment on resource-constrained edge devices. (4) Unlike Langsplat [50] and latentsplat [74], our current framework does not embed latent or semantic features into each STAG, necessitating integration with other pre-trained models during inference for high-level vision tasks such as editing and reasoning. However, future work could explore distilling rich visual features (e.g., SAM, CLIP) into our STAG representation and adapting our representation paradigm for video reasoning and generation tasks.

Table 4. Model Configuration of NutWorld

Parameter	Value
Encoder	
Input Resolution	288×512
Input Channels	RGB (3) + Depth (1)
Patch Size	16
Hidden Dimension	768
Attention Layers	10
Attention Heads	12
Window Size	3456
Positional Embedding	None
Upsampler Block	
Scale Factor	2
Decoder Ratio	2.0 / 3.0
Channel Width Decay	$768 \rightarrow 64$
Attention Layers per Block	2
Window Size	3456
Number of Blocks	4
STAG Decoder	
MLP Dimension	1024
Hidden Layers	1
Position Activation	None
Dynamic Activation	<i>tanh</i>
Scale Activation	<i>Softplus</i>
Rotation Activation	<i>Normalize</i>
Opacity Activation	<i>Sigmoid</i>
Color Activation	<i>Sigmoid</i>
Training Details	
Optimizer	AdamW
Learning Rate	1×10^{-4}
Weight Decay	0.05
Warm-Up Ratio	0.04
Batch Size	4
Number of GPUs	32
Total Epochs	100
Input Frames	6
Output Frames	10
Mixed Precision	bf16
Loss Weights	
λ_{MSE}	0.5
λ_{depth}	0.001
λ_{flow}	0.2

Video Reconstruction

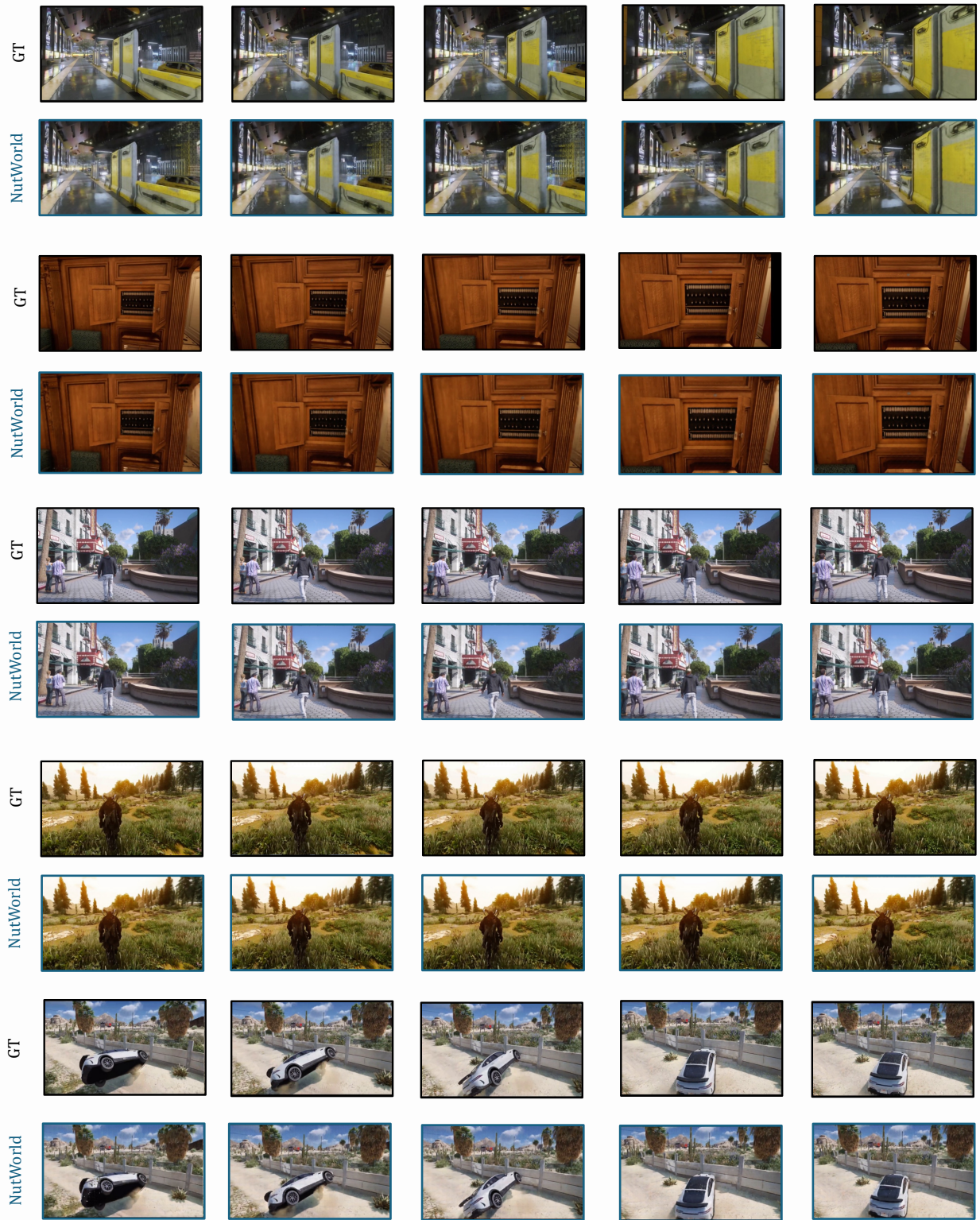


Figure 7. More qualitative results on video reconstruction.



Figure 8. More qualitative results on video editing.

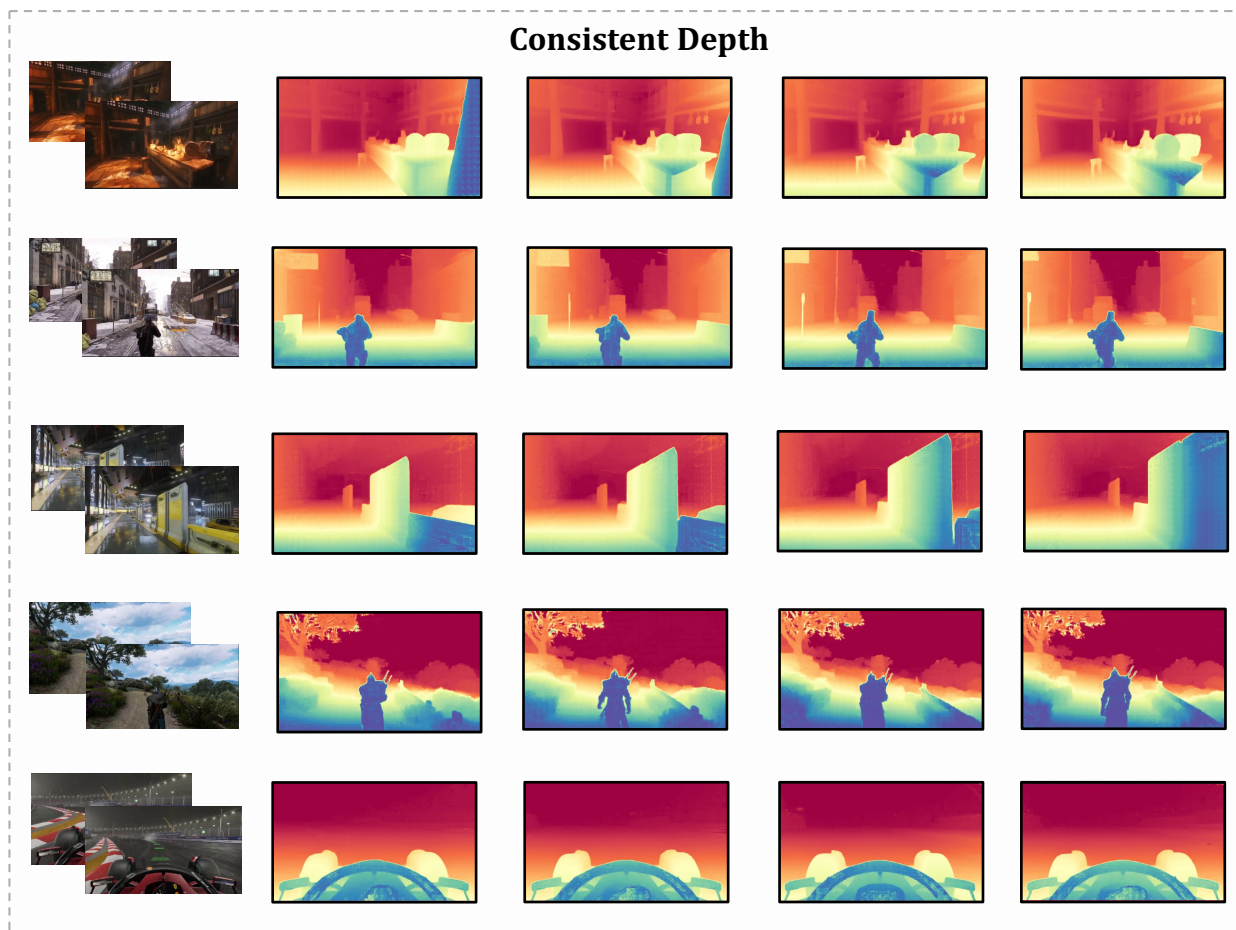


Figure 9. More qualitative results on consistent depth prediction.



Figure 10. More qualitative results on frame interpolation. Note that **Red Frame** denotes the interpolated frame.

Novel View Synthesis

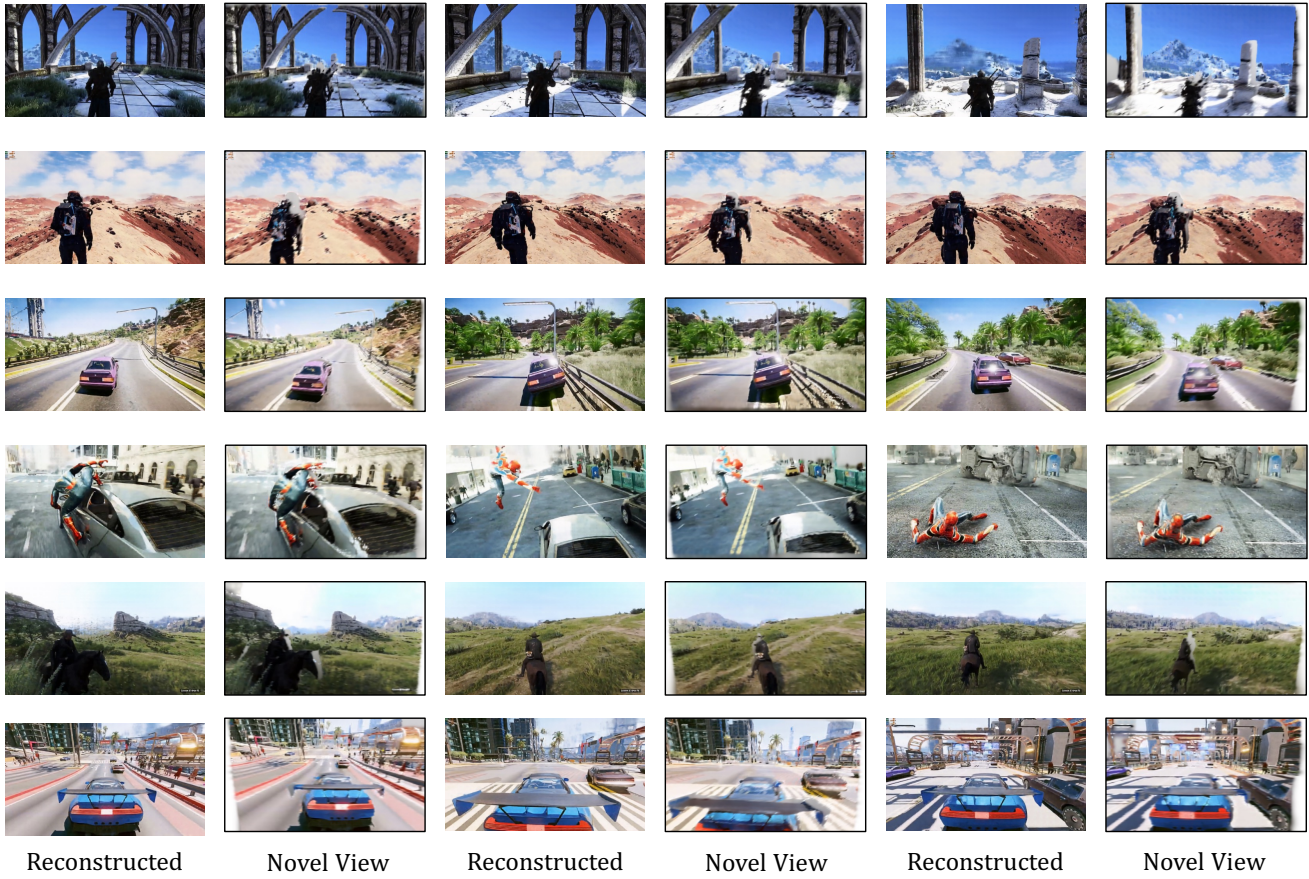


Figure 11. Qualitative results on novel view synthesis.



Figure 12. Qualitative results on video object segmentation.

References

- [1] Jinbin Bai, Tian Ye, Wei Chow, Enxin Song, Qing-Guo Chen, Xiangtai Li, Zhen Dong, Lei Zhu, and Shuicheng Yan. Meissonic: Revitalizing masked generative transformers for efficient high-resolution text-to-image synthesis. *arXiv preprint arXiv:2410.08261*, 2024. 4
- [2] Fan Bao, Chendong Xiang, Gang Yue, Guande He, Hongzhou Zhu, Kaiwen Zheng, Min Zhao, Shilong Liu, Yaole Wang, and Jun Zhu. Vidu: a highly consistent, dynamic and skilled text-to-video generator with diffusion models. *arXiv preprint arXiv:2405.04233*, 2024. 2
- [3] Shariq Farooq Bhat, Reiner Birkel, Diana Wofk, Peter Wonka, and Matthias Müller. Zoedepth: Zero-shot transfer by combining relative and metric depth. *arXiv preprint arXiv:2302.12288*, 2023. 5
- [4] Wenjing Bian, Zirui Wang, Kejie Li, Jia-Wang Bian, and Victor Adrian Prisacariu. Nope-nerf: Optimising neural radiance field with no pose prior. In *Proceedings of the IEEE/CVF Conference on Computer Vision and Pattern Recognition*, pages 4160–4169, 2023. 2
- [5] Alan C Bovik. *The essential guide to video processing*. Academic Press, 2009. 2
- [6] Ang Cao and Justin Johnson. Hexplane: A fast representation for dynamic scenes. In *Proceedings of the IEEE/CVF Conference on Computer Vision and Pattern Recognition*, pages 130–141, 2023. 3
- [7] Duygu Ceylan, Chun-Hao P Huang, and Niloy J Mitra. Pix2video: Video editing using image diffusion. In *Proceedings of the IEEE/CVF International Conference on Computer Vision*, pages 23206–23217, 2023. 2
- [8] David Charatan, Sizhe Lester Li, Andrea Tagliasacchi, and Vincent Sitzmann. pixelsplat: 3d gaussian splats from image pairs for scalable generalizable 3d reconstruction. In *CVPR*, pages 19457–19467, 2024. 3, 4, 5, 6, 10, 11
- [9] Yuedong Chen, Haoifei Xu, Chuanxia Zheng, Bohan Zhuang, Marc Pollefeys, Andreas Geiger, Tat-Jen Cham, and Jianfei Cai. Mvsplat: Efficient 3d gaussian splatting from sparse multi-view images. In *European Conference on Computer Vision*, pages 370–386. Springer, 2025. 3, 6, 11
- [10] Jaeyoung Chung, Jeongtaek Oh, and Kyoung Mu Lee. Depth-regularized optimization for 3d gaussian splatting in few-shot images. In *Proceedings of the IEEE/CVF Conference on Computer Vision and Pattern Recognition*, pages 811–820, 2024. 2
- [11] Tri Dao. Flashattention-2: Faster attention with better parallelism and work partitioning. *arXiv preprint arXiv:2307.08691*, 2023. 6
- [12] Tri Dao and Albert Gu. Transformers are SSMS: Generalized models and efficient algorithms through structured state space duality. In *International Conference on Machine Learning (ICML)*, 2024. 3
- [13] Tri Dao, Dan Fu, Stefano Ermon, Atri Rudra, and Christopher Ré. Flashattention: Fast and memory-efficient exact attention with io-awareness. *Advances in Neural Information Processing Systems*, 35:16344–16359, 2022. 6
- [14] Jiong Dong, Kaoru Ota, and Mianxiong Dong. Video frame interpolation: A comprehensive survey. *ACM Transactions on Multimedia Computing, Communications and Applications*, 19(2s):1–31, 2023. 2
- [15] Alexey Dosovitskiy. An image is worth 16x16 words: Transformers for image recognition at scale. *arXiv preprint arXiv:2010.11929*, 2020. 4
- [16] Yuanxing Duan, Fangyin Wei, Qiyu Dai, Yuhang He, Wenzheng Chen, and Baoquan Chen. 4d gaussian splatting: Towards efficient novel view synthesis for dynamic scenes. *arXiv preprint arXiv:2402.03307*, 2024. 2, 3
- [17] Christoph Feichtenhofer, Haoqi Fan, Jitendra Malik, and Kaiming He. Slowfast networks for video recognition. In *Proceedings of the IEEE/CVF international conference on computer vision*, pages 6202–6211, 2019. 2
- [18] Tsu-Jui Fu, Wenze Hu, Xianzhi Du, William Yang Wang, Yinfei Yang, and Zhe Gan. Guiding instruction-based image editing via multimodal large language models. *arXiv preprint arXiv:2309.17102*, 2023. 8
- [19] Yang Fu, Sifei Liu, Amey Kulkarni, Jan Kautz, Alexei A. Efros, and Xiaolong Wang. Colmap-free 3d gaussian splatting. In *Proceedings of the IEEE/CVF Conference on Computer Vision and Pattern Recognition (CVPR)*, pages 20796–20805, 2024. 2
- [20] Shenyuan Gao, Jiazhi Yang, Li Chen, Kashyap Chitta, Yihang Qiu, Andreas Geiger, Jun Zhang, and Hongyang Li. Vista: A generalizable driving world model with high fidelity and versatile controllability. *arXiv preprint arXiv:2405.17398*, 2024. 2
- [21] Yihui He, Rui Yan, Katerina Fragkiadaki, and Shoou-I Yu. Epipolar transformers. In *Proceedings of the IEEE/CVF conference on computer vision and pattern recognition*, pages 7779–7788, 2020. 3
- [22] Xu Hu, Yuxi Wang, Lue Fan, Junsong Fan, Junran Peng, Zhen Lei, Qing Li, and Zhaoxiang Zhang. Semantic anything in 3d gaussians. *arXiv preprint arXiv:2401.17857*, 2024. 8
- [23] Binbin Huang, Zehao Yu, Anpei Chen, Andreas Geiger, and Shenghua Gao. 2d gaussian splatting for geometrically accurate radiance fields. In *ACM SIGGRAPH 2024 Conference Papers*, pages 1–11, 2024. 2
- [24] Wenlong Huang, Chen Wang, Ruohan Zhang, Yunzhu Li, Jiajun Wu, and Li Fei-Fei. Voxposer: Composable 3d value maps for robotic manipulation with language models. *arXiv preprint arXiv:2307.05973*, 2023. 2
- [25] Wenlong Huang, Chen Wang, Yunzhu Li, Ruohan Zhang, and Li Fei-Fei. Rekep: Spatio-temporal reasoning of relational keypoint constraints for robotic manipulation. *arXiv preprint arXiv:2409.01652*, 2024. 2
- [26] Xuan Ju, Yiming Gao, Zhaoyang Zhang, Ziyang Yuan, Xintao Wang, Ailing Zeng, Yu Xiong, Qiang Xu, and Ying Shan. Miradata: A large-scale video dataset with long durations and structured captions, 2024. 2, 6, 11
- [27] Nikita Karaev, Ignacio Rocco, Benjamin Graham, Natalia Neverova, Andrea Vedaldi, and Christian Rupprecht. Co-tracker: It is better to track together. *arXiv preprint arXiv:2307.07635*, 2023. 2
- [28] Kai Katsumata, Duc Minh Vo, and Hideki Nakayama. A compact dynamic 3d gaussian representation for real-time dynamic view synthesis. In *European Conference on Computer Vision*, pages 394–412. Springer, 2025. 2, 3

- [29] Bernhard Kerbl, Georgios Kopanas, Thomas Leimkühler, and George Drettakis. 3d gaussian splatting for real-time radiance field rendering. *ACM Trans. Graph.*, 42(4):139–1, 2023. 2, 3
- [30] Alexander Kirillov, Eric Mintun, Nikhila Ravi, Hanzi Mao, Chloe Rolland, Laura Gustafson, Tete Xiao, Spencer Whitehead, Alexander C Berg, Wan-Yen Lo, et al. Segment anything. In *Proceedings of the IEEE/CVF International Conference on Computer Vision*, pages 4015–4026, 2023. 8
- [31] Dan Kondratyuk, Lijun Yu, Xiuye Gu, José Lezama, Jonathan Huang, Grant Schindler, Rachel Hornung, Vignesh Birodkar, Jimmy Yan, Ming-Chang Chiu, et al. Videopoet: A large language model for zero-shot video generation. *arXiv preprint arXiv:2312.14125*, 2023. 2
- [32] Agelos Kratimenos, Jiahui Lei, and Kostas Daniilidis. Dynmf: Neural motion factorization for real-time dynamic view synthesis with 3d gaussian splatting. In *European Conference on Computer Vision*, pages 252–269. Springer, 2025. 2, 3
- [33] Jiahui Lei, Yijia Weng, Adam Harley, Leonidas Guibas, and Kostas Daniilidis. Mosca: Dynamic gaussian fusion from casual videos via 4d motion scaffolds. *arXiv preprint arXiv:2405.17421*, 2024. 3
- [34] Hao Li, Jingfeng Li, Dingwen Zhang, Chenming Wu, Jieqi Shi, Chen Zhao, Haocheng Feng, Errui Ding, Jingdong Wang, and Junwei Han. Vdg: Vision-only dynamic gaussian for driving simulation. *arXiv preprint arXiv:2406.18198*, 2024. 2
- [35] Chen-Hsuan Lin, Wei-Chiu Ma, Antonio Torralba, and Simon Lucey. Barf: Bundle-adjusting neural radiance fields. In *Proceedings of the IEEE/CVF international conference on computer vision*, pages 5741–5751, 2021. 2
- [36] Lu Ling, Yichen Sheng, Zhi Tu, Wentian Zhao, Cheng Xin, Kun Wan, Lantao Yu, Qianyu Guo, Zixun Yu, Yawen Lu, et al. D13dv-10k: A large-scale scene dataset for deep learning-based 3d vision. In *Proceedings of the IEEE/CVF Conference on Computer Vision and Pattern Recognition*, pages 22160–22169, 2024. 3
- [37] Andrew Liu, Richard Tucker, Varun Jampani, Ameesh Makadia, Noah Snavely, and Angjoo Kanazawa. Infinite nature: Perpetual view generation of natural scenes from a single image. In *Proceedings of the IEEE/CVF International Conference on Computer Vision*, pages 14458–14467, 2021. 3
- [38] Yu-Lun Liu, Chen Gao, Andreas Meuleman, Hung-Yu Tseng, Ayush Saraf, Changil Kim, Yung-Yu Chuang, Johannes Kopf, and Jia-Bin Huang. Robust dynamic radiance fields. In *Proceedings of the IEEE/CVF Conference on Computer Vision and Pattern Recognition*, pages 13–23, 2023. 6, 7
- [39] Liying Lu, Ruizheng Wu, Huaijia Lin, Jiangbo Lu, and Jiaya Jia. Video frame interpolation with transformer. In *Proceedings of the IEEE/CVF Conference on Computer Vision and Pattern Recognition*, pages 3532–3542, 2022. 2
- [40] Ben Mildenhall, Pratul P Srinivasan, Matthew Tancik, Jonathan T Barron, Ravi Ramamoorthi, and Ren Ng. Nerf: Representing scenes as neural radiance fields for view synthesis. *Communications of the ACM*, 65(1):99–106, 2021. 2, 3
- [41] Thomas Müller, Alex Evans, Christoph Schied, and Alexander Keller. Instant neural graphics primitives with a multiresolution hash encoding. *ACM transactions on graphics (TOG)*, 41(4):1–15, 2022. 3
- [42] Richard A Newcombe, Dieter Fox, and Steven M Seitz. Dynamicfusion: Reconstruction and tracking of non-rigid scenes in real-time. In *Proceedings of the IEEE conference on computer vision and pattern recognition*, pages 343–352, 2015. 2
- [43] Abby O’Neill, Abdul Rehman, Abhinav Gupta, Abhiram Maddukuri, Abhishek Gupta, Abhishek Padalkar, Abraham Lee, Acorn Pooley, Agrim Gupta, Ajay Mandlekar, et al. Open x-embodiment: Robotic learning datasets and rt-x models. *arXiv preprint arXiv:2310.08864*, 2023. 2
- [44] Hao Ouyang, Qiuyu Wang, Yuxi Xiao, Qingyan Bai, Juntao Zhang, Kecheng Zheng, Xiaowei Zhou, Qifeng Chen, and Yujun Shen. Codef: Content deformation fields for temporally consistent video processing. In *Proceedings of the IEEE/CVF Conference on Computer Vision and Pattern Recognition*, pages 8089–8099, 2024. 2, 6, 7, 8
- [45] Linfei Pan, Dániel Baráth, Marc Pollefeys, and Johannes L Schönberger. Global structure-from-motion revisited. In *European Conference on Computer Vision (ECCV)*, 2024. 3
- [46] Keunhong Park, Utkarsh Sinha, Jonathan T Barron, Sofien Bouaziz, Dan B Goldman, Steven M Seitz, and Ricardo Martin-Brualla. Nerfies: Deformable neural radiance fields. In *Proceedings of the IEEE/CVF International Conference on Computer Vision*, pages 5865–5874, 2021. 3
- [47] Keunhong Park, Utkarsh Sinha, Peter Hedman, Jonathan T Barron, Sofien Bouaziz, Dan B Goldman, Ricardo Martin-Brualla, and Steven M Seitz. Hypernerf: A higher-dimensional representation for topologically varying neural radiance fields. *arXiv preprint arXiv:2106.13228*, 2021.
- [48] Albert Pumarola, Enric Corona, Gerard Pons-Moll, and Francesc Moreno-Noguer. D-nerf: Neural radiance fields for dynamic scenes. In *Proceedings of the IEEE/CVF Conference on Computer Vision and Pattern Recognition*, pages 10318–10327, 2021. 3
- [49] Chenyang Qi, Xiaodong Cun, Yong Zhang, Chenyang Lei, Xintao Wang, Ying Shan, and Qifeng Chen. Fatezero: Fusing attentions for zero-shot text-based video editing. In *Proceedings of the IEEE/CVF International Conference on Computer Vision*, pages 15932–15942, 2023. 2
- [50] Minghan Qin, Wanhua Li, Jiawei Zhou, Haoqian Wang, and Hanspeter Pfister. Langsplat: 3d language gaussian splatting. In *Proceedings of the IEEE/CVF Conference on Computer Vision and Pattern Recognition*, pages 20051–20060, 2024. 11
- [51] Alec Radford, Jong Wook Kim, Chris Hallacy, Aditya Ramesh, Gabriel Goh, Sandhini Agarwal, Girish Sastry, Amanda Askell, Pamela Mishkin, Jack Clark, et al. Learning transferable visual models from natural language supervision. In *International conference on machine learning*, pages 8748–8763. PMLR, 2021. 8
- [52] René Ranftl, Katrin Lasinger, David Hafner, Konrad Schindler, and Vladlen Koltun. Towards robust monocular

- depth estimation: Mixing datasets for zero-shot cross-dataset transfer. *IEEE transactions on pattern analysis and machine intelligence*, 44(3):1623–1637, 2020. 5
- [53] Jiawei Ren, Kevin Xie, Ashkan Mirzaei, Hanxue Liang, Xiaohui Zeng, Karsten Kreis, Ziwei Liu, Antonio Torralba, Sanja Fidler, Seung Wook Kim, et al. L4gm: Large 4d gaussian reconstruction model. *arXiv preprint arXiv:2406.10324*, 2024. 2, 8
- [54] Johannes L Schonberger and Jan-Michael Frahm. Structure-from-motion revisited. In *Proceedings of the IEEE conference on computer vision and pattern recognition*, pages 4104–4113, 2016. 2, 3
- [55] QiuHong Shen, Zike Wu, Xuanyu Yi, Pan Zhou, Hanwang Zhang, Shuicheng Yan, and Xinchao Wang. Gamba: Marry gaussian splatting with mamba for single view 3d reconstruction. *arXiv preprint arXiv:2403.18795*, 2024. 3
- [56] QiuHong Shen, Xingyi Yang, and Xinchao Wang. Flashsplat: 2d to 3d gaussian splatting segmentation solved optimally. In *European Conference on Computer Vision*, pages 456–472. Springer, 2025. 8
- [57] Wenzhe Shi, Jose Caballero, Ferenc Huszár, Johannes Totz, Andrew P Aitken, Rob Bishop, Daniel Rueckert, and Zehan Wang. Real-time single image and video super-resolution using an efficient sub-pixel convolutional neural network. In *Proceedings of the IEEE conference on computer vision and pattern recognition*, pages 1874–1883, 2016. 5
- [58] Vincent Sitzmann, Julien Martel, Alexander Bergman, David Lindell, and Gordon Wetzstein. Implicit neural representations with periodic activation functions. *Advances in neural information processing systems*, 33:7462–7473, 2020. 2
- [59] Nimit S Sohoni, Christopher R Aberger, Megan Leszczynski, Jian Zhang, and Christopher Ré. Low-memory neural network training: A technical report. *arXiv preprint arXiv:1904.10631*, 2019. 6
- [60] Deqing Sun, Xiaodong Yang, Ming-Yu Liu, and Jan Kautz. Pwc-net: Cnns for optical flow using pyramid, warping, and cost volume. In *Proceedings of the IEEE conference on computer vision and pattern recognition*, pages 8934–8943, 2018. 2
- [61] Rui Sun, Yumin Zhang, Tejal Shah, Jiahao Sun, Shuoying Zhang, Wenqi Li, Haoran Duan, Bo Wei, and Rajiv Ranjan. From sora what we can see: A survey of text-to-video generation. *arXiv preprint arXiv:2405.10674*, 2024. 2
- [62] Yang-Tian Sun, Yi-Hua Huang, Lin Ma, Xiaoyang Lyu, Yan-Pei Cao, and Xiaojuan Qi. Splatter a video: Video gaussian representation for versatile processing. *arXiv preprint arXiv:2406.13870*, 2024. 2, 3, 6, 7, 8, 11
- [63] Stanislaw Szymanowicz, Christian Ruppert, and Andrea Vedaldi. Splatter image: Ultra-fast single-view 3d reconstruction. In *Proceedings of the IEEE/CVF Conference on Computer Vision and Pattern Recognition*, pages 10208–10217, 2024. 4
- [64] Jiayang Tang, Zhaoxi Chen, Xiaokang Chen, Tengfei Wang, Gang Zeng, and Ziwei Liu. Lgm: Large multi-view gaussian model for high-resolution 3d content creation. In *European Conference on Computer Vision*, pages 1–18. Springer, 2025. 8, 10
- [65] A Murat Tekalp. *Digital video processing*. Prentice Hall Press, 2015. 2
- [66] Shimon Ullman. The interpretation of structure from motion. *Proceedings of the Royal Society of London. Series B. Biological Sciences*, 203(1153):405–426, 1979. 2, 3
- [67] A Vaswani. Attention is all you need. *Advances in Neural Information Processing Systems*, 2017. 3, 4
- [68] Jianyuan Wang, Nikita Karaev, Christian Ruppert, and David Novotny. Vggsfm: Visual geometry grounded deep structure from motion. In *Proceedings of the IEEE/CVF Conference on Computer Vision and Pattern Recognition*, pages 21686–21697, 2024. 3
- [69] Qianqian Wang, Vickie Ye, Hang Gao, Jake Austin, Zhengqi Li, and Angjoo Kanazawa. Shape of motion: 4d reconstruction from a single video. *arXiv preprint arXiv:2407.13764*, 2024. 2, 3
- [70] Shuzhe Wang, Vincent Leroy, Yohann Cabon, Boris Chidlovskii, and Jerome Revaud. Dust3r: Geometric 3d vision made easy. In *Proceedings of the IEEE/CVF Conference on Computer Vision and Pattern Recognition*, pages 20697–20709, 2024. 3
- [71] Shizun Wang, Xingyi Yang, QiuHong Shen, Zhenxiang Jiang, and Xinchao Wang. Gflow: Recovering 4d world from monocular video. *arXiv preprint arXiv:2405.18426*, 2024. 3
- [72] Xiaofeng Wang, Zheng Zhu, Guan Huang, Fangbo Qin, Yun Ye, Yijia He, Xu Chi, and Xingang Wang. Mvster: Epipolar transformer for efficient multi-view stereo. In *European Conference on Computer Vision*, pages 573–591. Springer, 2022. 3
- [73] Zirui Wang, Shangzhe Wu, Weidi Xie, Min Chen, and Victor Adrian Prisacariu. Nerf-: Neural radiance fields without known camera parameters. *arXiv preprint arXiv:2102.07064*, 2021. 2
- [74] Christopher Wewer, Kevin Raj, Eddy Ilg, Bernt Schiele, and Jan Eric Lenssen. latentsplat: Autoencoding variational gaussians for fast generalizable 3d reconstruction. *arXiv preprint arXiv:2403.16292*, 2024. 3, 11
- [75] GuanJun Wu, Taoran Yi, Jiemin Fang, Lingxi Xie, Xiaopeng Zhang, Wei Wei, Wenyu Liu, Qi Tian, and Xingang Wang. 4d gaussian splatting for real-time dynamic scene rendering. In *Proceedings of the IEEE/CVF Conference on Computer Vision and Pattern Recognition*, pages 20310–20320, 2024. 2, 3, 6, 7
- [76] Haofei Xu, Jing Zhang, Jianfei Cai, Hamid RezaTofighi, Fisher Yu, Dacheng Tao, and Andreas Geiger. Unifying flow, stereo and depth estimation. *IEEE Transactions on Pattern Analysis and Machine Intelligence*, 2023. 2, 5
- [77] Yinghao Xu, Zifan Shi, Wang Yifan, Hansheng Chen, Ceyuan Yang, Sida Peng, Yujun Shen, and Gordon Wetzstein. Grm: Large gaussian reconstruction model for efficient 3d reconstruction and generation. *arXiv preprint arXiv:2403.14621*, 2024. 4, 10
- [78] Lihe Yang, Bingyi Kang, Zilong Huang, Zhen Zhao, Xiaogang Xu, Jiashi Feng, and Hengshuang Zhao. Depth anything v2. *arXiv preprint arXiv:2406.09414*, 2024. 2, 4, 5
- [79] Zeyu Yang, Hongye Yang, Zijie Pan, and Li Zhang. Real-time photorealistic dynamic scene representation and

- rendering with 4d gaussian splatting. *arXiv preprint arXiv:2310.10642*, 2023. 2, 3
- [80] Ziyi Yang, Xinyu Gao, Wen Zhou, Shaohui Jiao, Yuqing Zhang, and Xiaogang Jin. Deformable 3d gaussians for high-fidelity monocular dynamic scene reconstruction. In *Proceedings of the IEEE/CVF Conference on Computer Vision and Pattern Recognition*, pages 20331–20341, 2024. 2, 3
- [81] Botao Ye, Hong Chang, Bingpeng Ma, Shiguang Shan, and Xilin Chen. Joint feature learning and relation modeling for tracking: A one-stream framework. In *ECCV*, 2022. 2
- [82] Vickie Ye, Zhengqi Li, Richard Tucker, Angjoo Kanazawa, and Noah Snavely. Deformable sprites for unsupervised video decomposition. In *Proceedings of the IEEE/CVF Conference on Computer Vision and Pattern Recognition*, pages 2657–2666, 2022. 2
- [83] Xuanyu Yi, Jiajun Deng, Qianru Sun, Xian-Sheng Hua, Joo-Hwee Lim, and Hanwang Zhang. Invariant training 2d-3d joint hard samples for few-shot point cloud recognition. In *Proceedings of the IEEE/CVF International Conference on Computer Vision*, pages 14463–14474, 2023. 11
- [84] Xuanyu Yi, Zike Wu, Qihong Shen, Qingshan Xu, Pan Zhou, Joo-Hwee Lim, Shuicheng Yan, Xinchao Wang, and Hanwang Zhang. Mvgamba: Unify 3d content generation as state space sequence modeling. *arXiv preprint arXiv:2406.06367*, 2024. 3
- [85] Xuanyu Yi, Zike Wu, Qingshan Xu, Pan Zhou, Joo-Hwee Lim, and Hanwang Zhang. Diffusion time-step curriculum for one image to 3d generation. In *Proceedings of the IEEE/CVF Conference on Computer Vision and Pattern Recognition*, pages 9948–9958, 2024. 2
- [86] Alex Yu, Vickie Ye, Matthew Tancik, and Angjoo Kanazawa. pixelnerf: Neural radiance fields from one or few images. In *Proceedings of the IEEE/CVF conference on computer vision and pattern recognition*, pages 4578–4587, 2021. 2
- [87] Zehao Yu, Anpei Chen, Binbin Huang, Torsten Sattler, and Andreas Geiger. Mip-splatting: Alias-free 3d gaussian splatting. In *Proceedings of the IEEE/CVF Conference on Computer Vision and Pattern Recognition*, pages 19447–19456, 2024. 2
- [88] Zehao Yu, Torsten Sattler, and Andreas Geiger. Gaussian opacity fields: Efficient and compact surface reconstruction in unbounded scenes. *arXiv preprint arXiv:2404.10772*, 2024. 2
- [89] Pedram Zamirai, Jian Zhang, Christopher R Aberger, and Christopher De Sa. Revisiting bfloat16 training. *arXiv preprint arXiv:2010.06192*, 2020. 6
- [90] Chuanrui Zhang, Yingshuang Zou, Zhuoling Li, Minmin Yi, and Haoqian Wang. Transplat: Generalizable 3d gaussian splatting from sparse multi-view images with transformers. *arXiv preprint arXiv:2408.13770*, 2024. 3, 6, 11
- [91] Hong-Bo Zhang, Yi-Xiang Zhang, Bineng Zhong, Qing Lei, Lijie Yang, Ji-Xiang Du, and Duan-Sheng Chen. A comprehensive survey of vision-based human action recognition methods. *Sensors*, 19(5):1005, 2019. 2
- [92] Kai Zhang, Sai Bi, Hao Tan, Yuanbo Xiangli, Nanxuan Zhao, Kalyan Sunkavalli, and Zexiang Xu. Gs-irm: Large reconstruction model for 3d gaussian splatting. In *European Conference on Computer Vision*, pages 1–19. Springer, 2025. 3, 4
- [93] Richard Zhang, Phillip Isola, Alexei A Efros, Eli Shechtman, and Oliver Wang. The unreasonable effectiveness of deep features as a perceptual metric. In *CVPR*, 2018. 7
- [94] Tinghui Zhou, Richard Tucker, John Flynn, Graham Fyffe, and Noah Snavely. Stereo magnification: Learning view synthesis using multiplane images. *arXiv preprint arXiv:1805.09817*, 2018. 2, 3, 6, 11
- [95] Zehao Zhu, Zhiwen Fan, Yifan Jiang, and Zhangyang Wang. Fsgs: Real-time few-shot view synthesis using gaussian splatting. In *European Conference on Computer Vision*, pages 145–163. Springer, 2025. 2
- [96] Chen Ziwen, Hao Tan, Kai Zhang, Sai Bi, Fujun Luan, Yicong Hong, Li Fuxin, and Zexiang Xu. Long-irm: Long-sequence large reconstruction model for wide-coverage gaussian splats. *arXiv preprint arXiv:2410.12781*, 2024. 3
- [97] Matthias Zwicker, Hanspeter Pfister, Jeroen Van Baar, and Markus Gross. Ewa splatting. *IEEE Transactions on Visualization and Computer Graphics*, 8(3):223–238, 2002. 10